Supplemental Information

Inventory of Supplemental Materials:

Figure S1, related to Figure 2. The autophagy pathway is required for SNB-1 localization in AIY and during early development to instruct AIY presynaptic assembly.

Figure S2, related to Figure 2. Examination of additional autophagy mutant alleles, including genes that regulate selective autophagy.

Figure S3, related to Figure 3. Autophagy genes are expressed in neurons, including AIY, and active zone localization is disrupted in autophagy mutants.

Figure S4, related to Figure 4. Autophagy pathway mutants do not affect glia morphology or subcellular localization of UNC-40/DCC and MIG-10B/Lamellipodin.

Figure S5, related to Figure 5. UNC-104/KIF1A is required for autophagosome accumulation at AIY presynaptic regions in late autophagy mutants.

Figure S6, related to Figure 7. The autophagy pathway is required for neurodevelopment in some, but not all neurons in *C. elegans*.

Table S1, related to Figure 2. Annotated list of autophagy genes examined in this study.

Movie S1, related to Figure 5. Time-lapse video of GFP::LGG-1, AV biogenesis in AIY.

Movie S2, related to Figure 5. Time-lapse video of GFP::LGG-1, AV biogenesis in AIY.

Movie S3, related to Figure 5. Time-lapse video of GFP::LGG-1, AV biogenesis in AIY.

Movie S4, related to Figure 5. Time-lapse video of GFP::LGG-1, AV retrograde trafficking in AIY.

Supplemental Experimental Procedures

Supplemental References

Supplemental Figures and Legends:
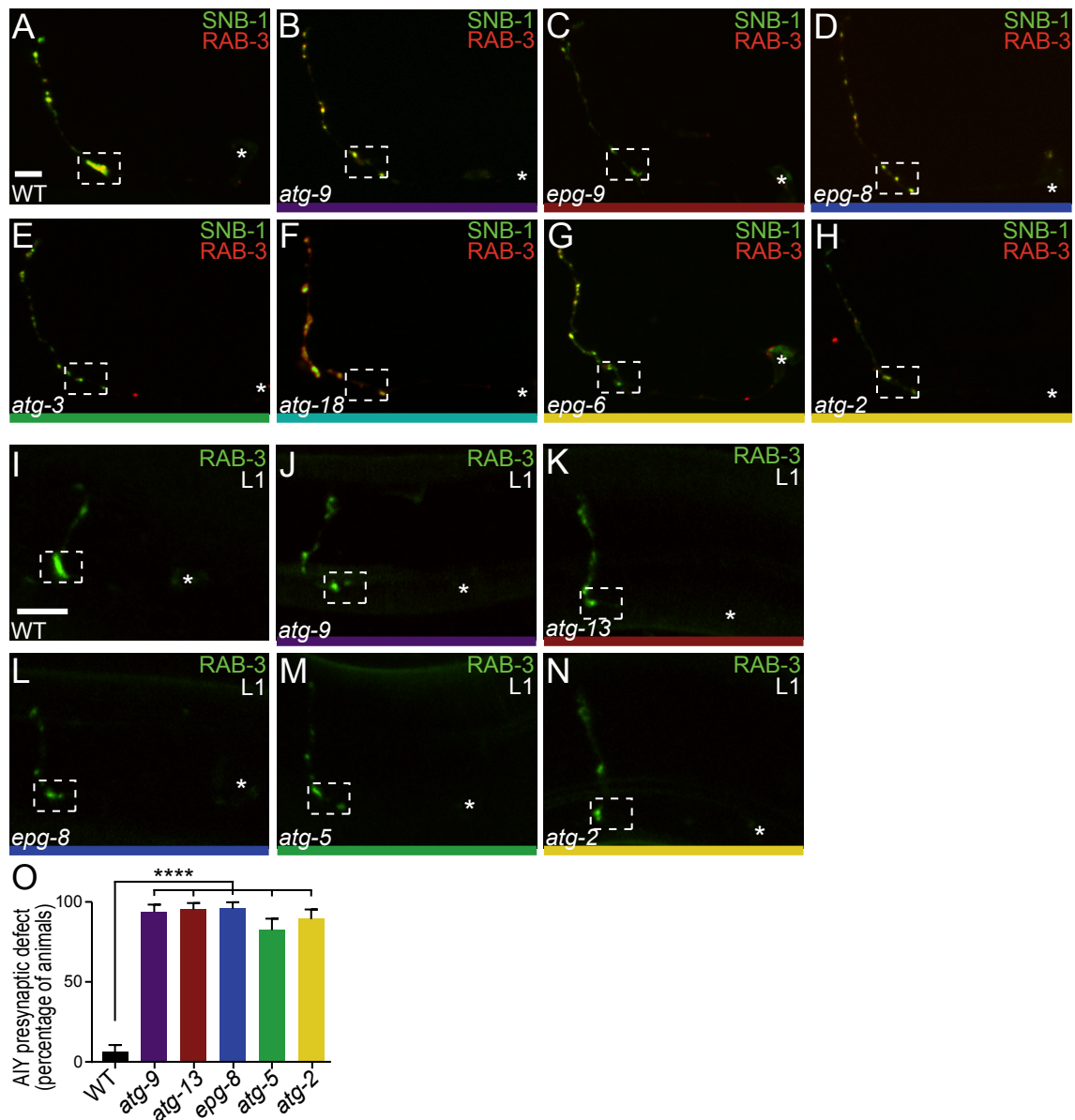
Figure S1

Figure S1. The autophagy pathway is required for SNB-1 localization in AIY and during early development to instruct AIY presynaptic assembly, related to Figure 2.

(A-H) Distribution of synaptic vesicles (visualized with SNB-1::YFP and mCh::RAB-3) in wild type (A), *atg-9(bp564)* (B), *epg-9(bp320)* (C), *epg-8(bp251)* (D), *atg-3(bp412)* (E), *atg-18(gk447069)* (F), *epg-6(bp242)* (G), and *atg-2(bp576)* (H) mutant animals. (I-N) Distribution of synaptic vesicles (visualized with GFP::RAB-3) in larval stage 1 (L1) wild type (I), *atg-9(bp564)* (J), *atg-13(bp414)* (K), *epg-8(bp251)* (L), *atg-5(bp484)* (M), and *atg-2(bp576)* (N) mutant animals. Note that similar to adult mutant animals (Figure 2), L1 autophagy mutant animals display AIY presynaptic defects. We also note that in longitudinal studies, we observe that the synaptic phenotypes that emerged in the L1 stage not did deteriorate as animals progressed through development (data not shown). (O) Quantification of the AIY presynaptic defect in wild type and autophagy pathway mutant L1 animals. Error bars

represent 95% confidence interval. ****, P< 0.0001 between indicated groups by Fisher's exact test. Each image is a maximal projection of a confocal z-stack; the asterisk denotes the location of the cell body and the dashed box encloses AIY Zone 2. Scale bars (in A for A-H; in I for I-N), 5 μm.
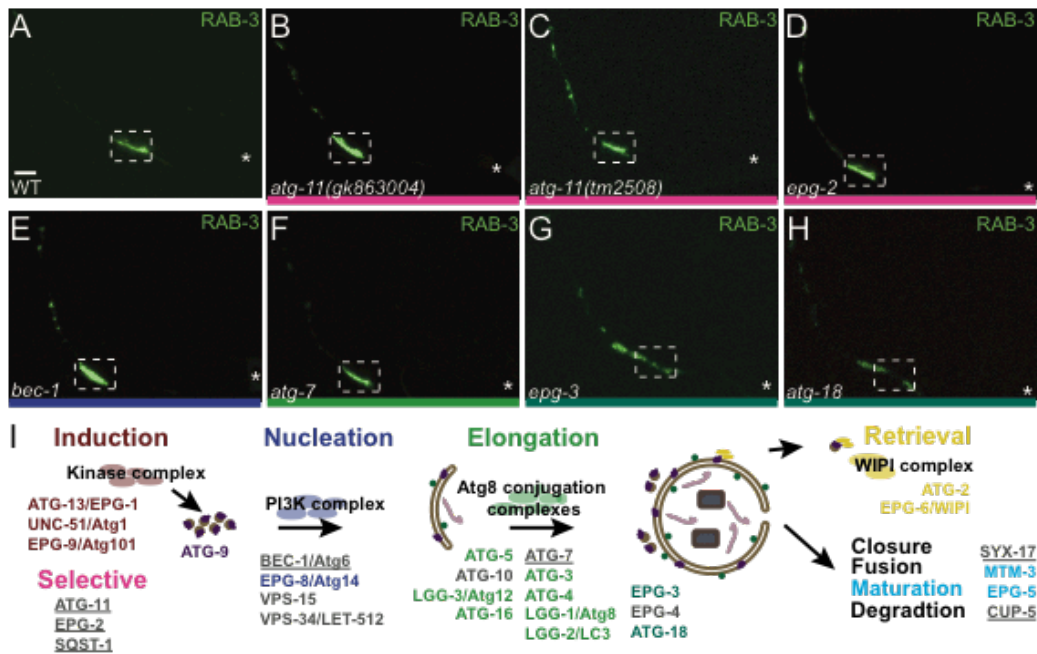
Figure S2

Figure S2. Examination of additional autophagy mutant alleles, including genes that regulate selective autophagy, related to Figure 2.

(A-F) Distribution of synaptic vesicles (visualized with GFP::RAB-3) in wild type (A), *atg-11(gk863004)* (B), *atg-11(tm2508)* (C), *epg-2(gk104842)* (D), *bec-1(ok691)* (E), and *atg-7(bp422)* (F), mutant animals. Note that these alleles do not display presynaptic defects in AIY. (G-H) Distribution of synaptic vesicles (visualized with GFP::RAB-3) in *epg-3(tm5475)* (G) and *atg-18(gk447069)* (H) mutant animals. Note that *epg-3* and *atg-18* mutants display presynaptic defects (85% of *epg-3* mutant animals, n=111 and 95% of *atg-18* mutant animals, n=119). EPG-3/VMP1 and ATG-18/WIPI1/2 regulate downstream steps of autophagosome elongation (Lu et al., 2011; Obara et al., 2008; Polson et al., 2010; Tian et al., 2010). Each image is a maximal projection of a confocal z-stack; the asterisk denotes the location of the cell body and the dashed box encloses AIY Zone 2. Scale bar (in A for A-H), 5 μm. (I) Diagram illustrating the autophagy pathway and listing the components of each step. Gray underlined genes were examined, with no detected AIY presynaptic defect. Gray genes that are not underlined were not examined due to lack of available alleles. All other colored gene names were examined and phenotypes were observed for AIY presynaptic assembly. ATG-11, EPG-2 and SQST-1 are part of the selective autophagy pathway (pink). The *bec-1(ok691)* allele is a balanced allele, and we hypothesize that examined escapers had maternal contribution of the wild type copy of the *bec-1* mRNA. A second *bec-1* allele (*gk202351*), which eliminates an early splice site in only one of the predicted *bec-1* isoforms, also did not display AIY presynaptic defects. The *atg-7(bp422)* allele is a putative hypomorph. SXY-17 is a purported ortholog of a SNARE that mediates fusion between autophagosomes and endosomes/lysosomes (Hegedus et al., 2013). The available *syx-17* alleles are missense alleles with no known effects on protein function. CUP-5/MLN1/TRPML1 is important for lysosome biogenesis and proteolytic degradation of autolysosomes in *C. elegans* (Treusch et al., 2004). The *cup-5* allele *ar465* has previously been observed to affect only some cell types and null alleles are lethal (Schaheen et al., 2006; Sun et al., 2011).
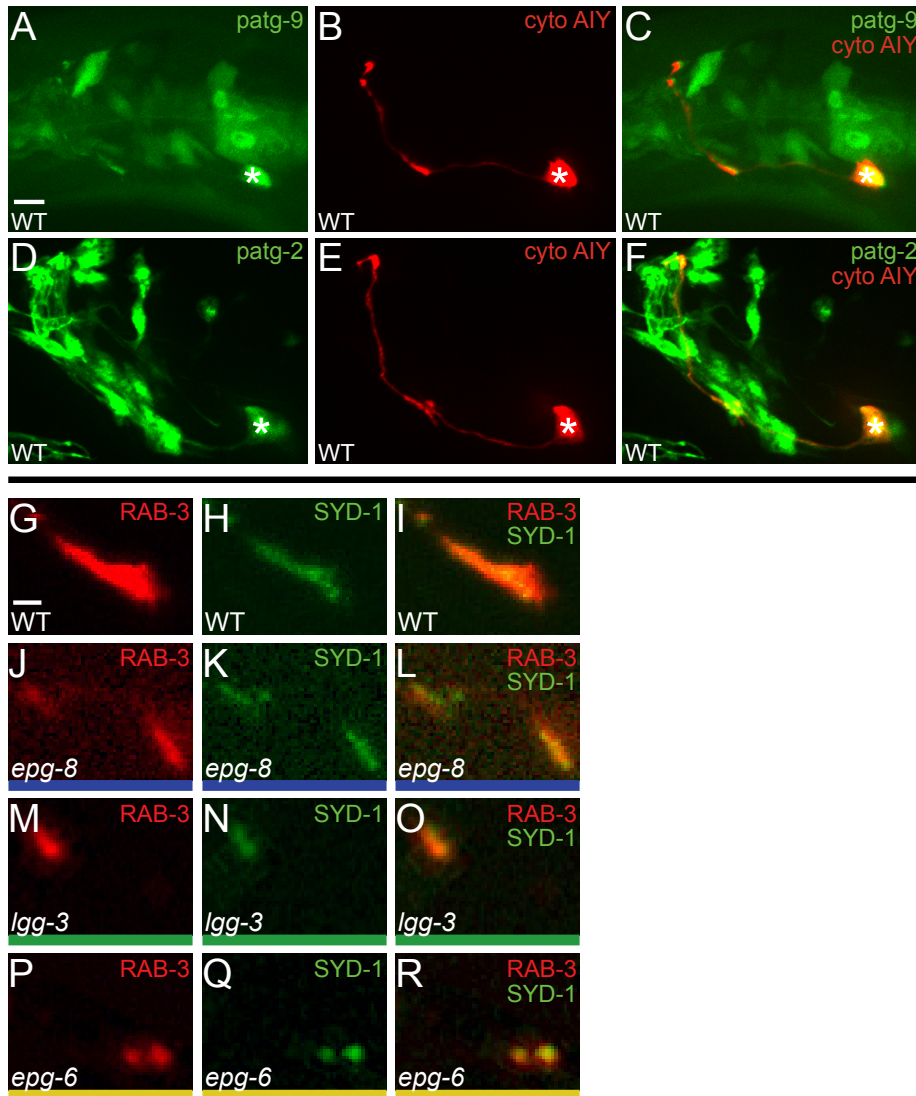
Figure S3

Figure S3. Autophagy genes are expressed in neurons, including AIY, and active zone localization is disrupted in autophagy mutants, related to Figure 3.
(A-F) Expression pattern of the autophagy genes *atg-9* (A-C) and *atg-2* (D-F) using transcriptional fusions (see Supplemental Experimental Procedures). AIY is identified with cytoplasmic mCh (B and E). (C and F) Merge images for (A-B) and (D-E), respectively. (G-R) Distribution of synaptic vesicles (visualized with mCh::RAB-3) and active zones (visualized with GFP::SYD-1) in Zone 2 of AIY in wild type (G-I), *epg-8(bp251)* (J-L), *lgg-3(tm1642)* (M-O), and *epg-6(bp242)* (P-R) mutant animals. Each image is a maximal projection of a confocal z-stack; the asterisk denotes the location of the cell body. Scale bar in A for A-F, 5 μm, and in G for G-R, 1 μm.
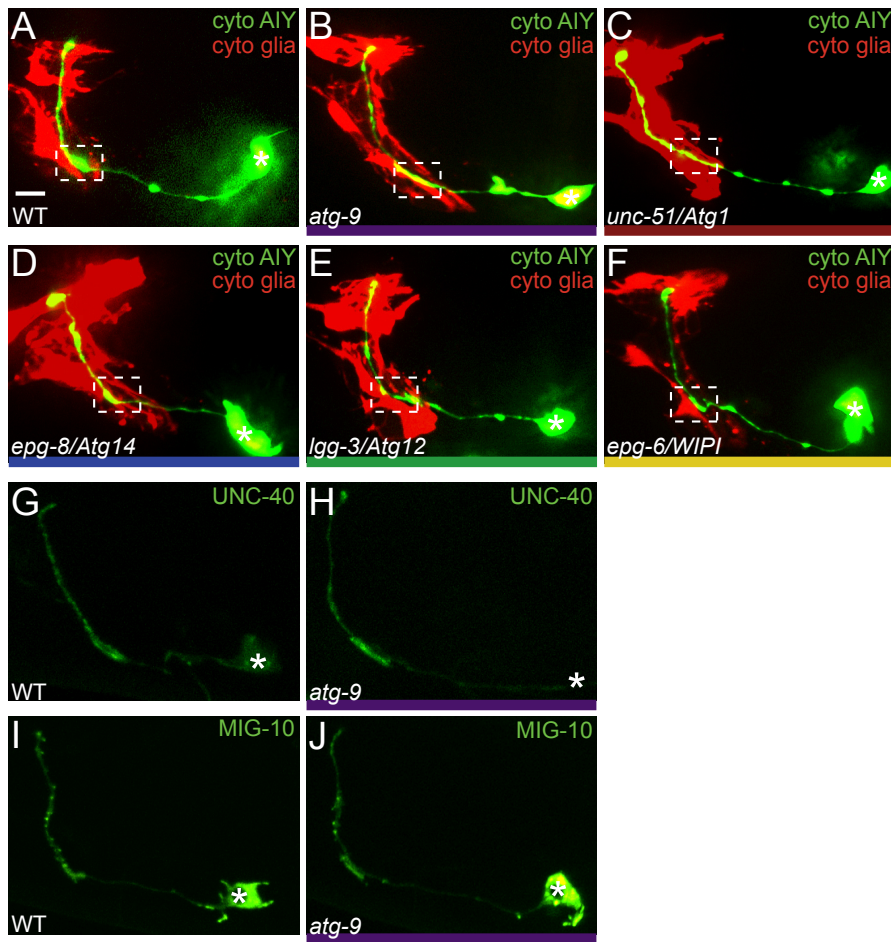
Figure S4

Figure S4. Autophagy pathway mutants do not affect glia morphology or subcellular localization of UNC-40/DCC and MIG-10B/Lamellipodin, related to Figure 4.
(A-F) Glia and AIY morphology in wild type (A), *atg-9(bp564)* (B), *unc-51(e369)* (C), *epg-8(bp251)* (D), *lgg-3(tm1642)* (E), and *epg-6 (bp242)* (F) mutant animals. Note that the glia makes close contact with AIY Zone 2 in all genetic backgrounds. This was confirmed by analyzing AIY-glia contact sites through GRASP (data not shown) (Feinberg et al., 2008; Shao et al., 2013). (G-J) Distribution of the Netrin receptor UNC-40 and downstream adaptor protein MIG-10B in AIY, visualized with UNC-40::GFP (G-H) and MIG-10B::GFP (I-J), respectively, in wild type (G and I) and *atg-9(wy56)* (H and J) mutant animals (Colón-Ramos et al., 2007; Stavoe et al., 2012). Note that both proteins are enriched in synaptic regions (Zones 2 and 3), but absent from Zone 1, in both wild type and *atg-9* mutant animals. Each image is a maximal projection of a confocal z-stack; the asterisk denotes the location of the cell body and the dashed box encloses AIY Zone 2. Scale bar in A for A-J, 5 μm.
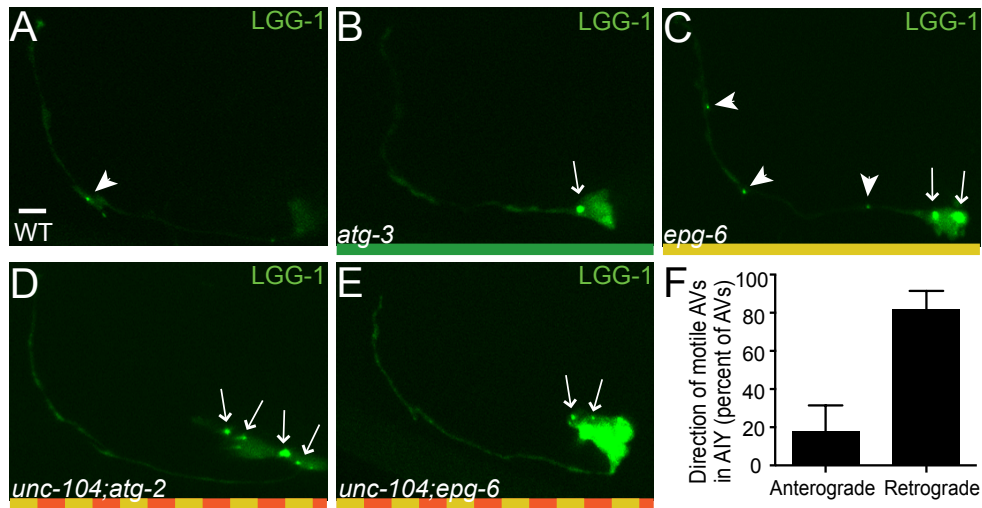
Figure S5

Figure S5. UNC-104/KIF1A is required for autophagosome accumulation at AIY presynaptic regions in late autophagy mutants, related to Figure 5.

(A-E) Distribution of autophagosomes (visualized with GFP::LGG-1) in AIY in wild type (A), *atg-3(bp412)* (B), *epg-6(bp424)* (C), *unc-104(e1265);atg-2(bp576)* (D), and *unc-104(e1265);epg-6(bp424)* (E) mutant and double mutant animals. Each image is a maximal projection of a confocal z-stack; arrowheads denote the location of LGG-1 puncta in the neurite and arrows denote the location of LGG-1 puncta in the cell body. Scale bar in A for A-E, 5 μm. (F) Quantification of the direction of movement of motile autophagosomes (AV) in the AIY neurite. Anterograde and retrograde describe puncta moving away from or toward the cell body, respectively. Of the GFP::LGG-1 puncta observed, 42% were motile and 58% were stationary or made small bidirectional movements (n=120). Quantifications were performed on 5 minute videos, with z-stacks captured at maximal speed (at least once every 10 seconds). Error bars represent 95% confidence interval.
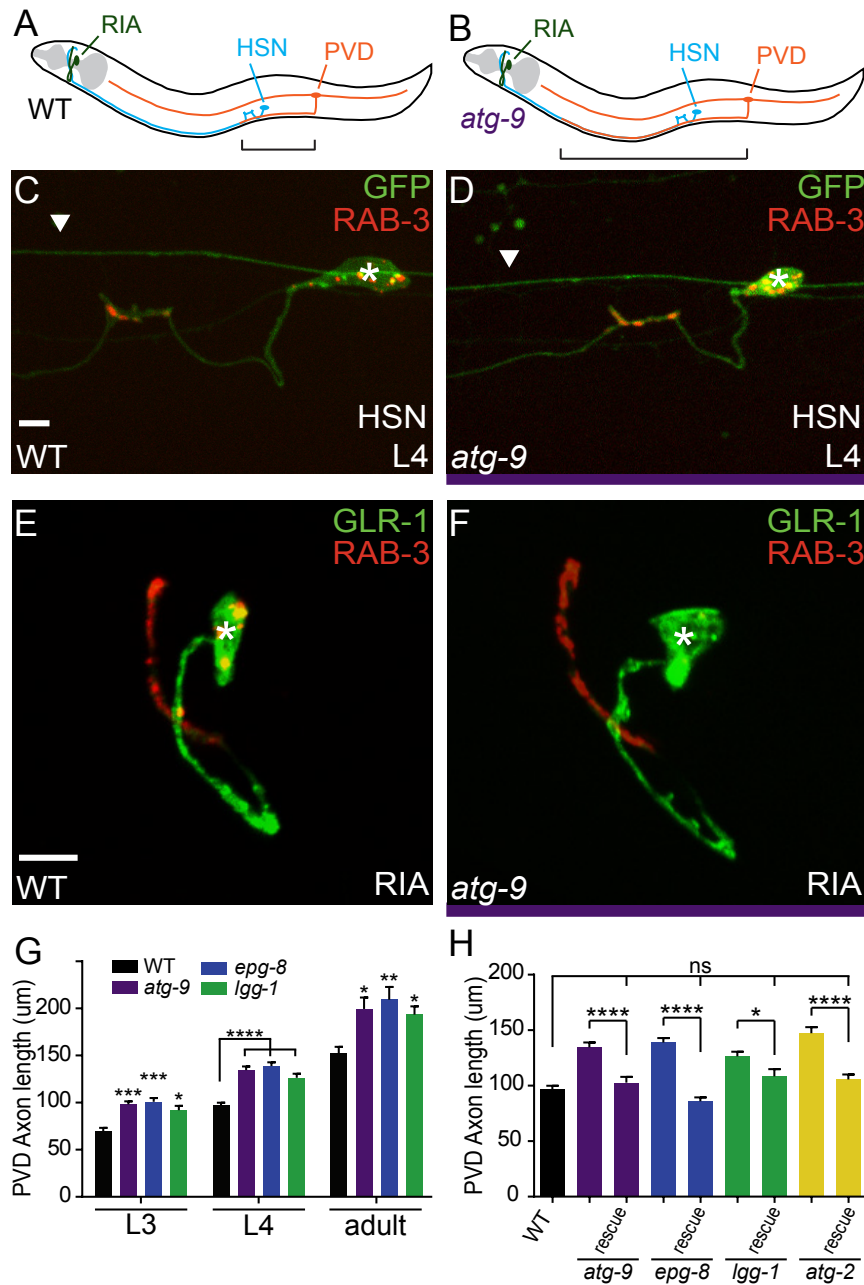
Figure S6

Figure S6. The autophagy pathway is required for neurodevelopment in some, but not all neurons in *C. elegans*, related to Figure 7.
(A-B) Schematics of the morphology of RIA (green), HSN (cyan) and PVD (orange) neurons in wild type (A) and *atg-9* mutant (B) L4 animals. (C-D) HSN morphology (visualized with cytoplasmic GFP) and distribution of synaptic vesicles (visualized with mCh::RAB-3) in wild type (C) and *atg-9(bp564)* mutant (D) L4 animals. Arrowhead indicates non-HSN neuronal process. We observed no significant differences in HSN axon morphology, axon guidance or localization of presynapses in autophagy mutants. (E-F) Distribution of synaptic vesicles (visualized with mCh::RAB-3) and postsynaptic specializations (visualized with GLR-1::GFP) in RIA in wild type (E) and *atg-9(bp564)* mutant (F) animals. We observed no significant differences in RIA neurite morphology,

neurite guidance or localization of pre- and postsynapses in autophagy mutants. We also examined neurons RIB, DA9 and NSM and did not observe phenotypes in the autophagy mutants (data not shown). (G) Quantification of PVD axon length in wild type and autophagy mutant L3, L4 and young adult animals. Note that PVD axon length is longer in autophagy mutant animals compared to wild type at all developmental stages. ****, P< 0.0001; ***, P< 0.001; **, P< 0.01; *, P< 0.05 between indicated mutant and wild type by one-way ANOVA with Tukey's post-hoc analysis. (H) Quantification of PVD axon length in wild type, autophagy mutants and autophagy mutants with rescue of the indicated genes (*atg-9, lgg-1*, and *atg-2* rescued with panneuronal expression; *epg-8* rescued using its endogenous promoter), all quantified in L4 animals. ****, P< 0.0001; *, P< 0.05 between indicated groups by Student's t-test. ns, not significant between wild type and rescued autophagy mutants by one-way ANOVA with Tukey's post-hoc analysis. Error bars represent standard error of the mean. Each image is a maximal projection of a confocal z-stack; the asterisk denotes the location of the cell body. Scale bars (in C for C-D, in E for E-F), 5 μm.

Table S1

		Yeast/Mammalian Name	Worm Name	Alleles	Lesion	Protein Effect	Genetic Sequence
Initiation	*	Atg1p	unc-51	e369	Not curated on WormBase		
	*	Atg101	epg-9	bp320	Q109, Q182, Q136 to ochre stop	Putative null	aaaaatgcgtCaacgcgtcgc
	*	Atg13p	atg-13/epg-1	bp414	Splice site - first exon/intron	Putative null	tataattcagGtatttataat
ATG-9	*	Atg9	atg-9	bp564	Q235 to stop	Putative null	tgccgacgatCagctgcccaa
	*			wy56	W513 to opal/umber stop	Putative null	cgtccacgtgGaagggaaagg
	*			gk421128	Q685 to stop	Putative null	gcagcagcagCagggtaaaat
Nucleation	*	Atg14	epg-8	bp251	W251, W170, W93 to opal/umber stop	Putative null	tcacaactgcCcaatttttcg
		Atg6/beclin	bec-1	gk202351	Splice site - first exon/intron	Putative null	aaaaaactcaCtttttctcg
				ok691	Deletion	Null, lethal	aataaattcaCAAT...TCTAatttttcgga
Elongation	*	Atg3p	atg-3	bp412	G32E	Potential hypomorph	cgtgaaaccgGagttctaaca
	*	Atg5p	atg-5	bp484	Splice site - first exon/intron	Putative null	aatacagaaaGttagattttc
	*	Atg12p	lgg-3	tm1642	Deletion	Putative null	ccttttcataAATCATCT...GAATAacatcgggat
	*	Atg8p	lgg-1	bp500	Q93 to ochre stop	Putative null	tggtagagttGtcccattgtg
	*	Atg8/LC3	lgg-2	tm5755	Deletion	Putative null	caggtatttaCATTTAAA...GTTATAtgctcgggt
	*	Atg4A/B	atg-4.1	gk127286	W254, W227 to opal/umber stop	Putative null	gaaggggacgCcattcgggga
		Atg4C/D	atg-4.2	gk430078	K84 to ochre stop	Putative null	gagcaaaattAaatcgtgagt
	*	Atg16	atg-16.1	gk668615	Q407 to ochre stop	Putative null	ctttgattttGaatatcccaa
			atg-16.2	gk145022	W253 to opal/umber stop	Putative null	catcagacatCcattcaacat
		Atg7p	atg-7	bp422	E291K	Hypomorph	cttaagtaaaGagttcgatcc
				tm2976	Deletion/Insertion	Null, lethal	cgacaacaacACATATT...ATAATATTtgaattttt
		Atg10	atg-10	bp588	very sick animals, not curated		
	*	VMP1	epg-3	tm5475	Deletion	Putative null	cgtggtgggTGTTGCTC...CGAGCGTCgtaaatct
	*	Atg18/WIPI1/2	atg-18	gk447069	Q79 to amber stop	Putative null	ggatccttctGagatataact
Retreival	*	Atg2p (ATG2A/B)	atg-2	bp576	W715 to opal/umber stop	Putative null	gctcaaattgGcaagttgatc
	*	Atg18/WIPI4	epg-6	bp242	R54, R161, R161, R129 to opal/umber stop	Putative null	tcttccgatcGgatttgttta
Fusion		STX17/syntaxin 17	syx-17	gk658736, gk789491, gk692217, gk506884, gk694538, gk384616, gk636669, gk781173, all missense alleles, see www.wormbase.org			
Maturation	*	MTMR3	mtm-3	tm4475	Deletion/Insertion	Putative null	agccgttttgAAGCAAAT...AATTATTAttattatt
	*	mEpg5	epg-5	tm3425	Deletion	Putative null	catattcaacTAGTAAGC...ACACTTGCggatgtt
Degradation		MLN1/TFPML1	cup-5	ar465	G419E, G401E, G397E	Hypomorph	attatcattgGaactgttgca
Selective		Atg11	atg-11	gk863004	R1145 to opal/umber stop	Putative null	gtcgagtctcCgatccggtgg
				tm2508	Deletion	Possible null	ttgaatcgaaTATGAA...GAAAGCAaaactggag
		Nematode-specific gene	epg-2	gk104842	Q484 to ochre stop	Putative null	tgctgctcatCaaagcttgag
		p62	sqst-1	ok2869	Deletion	Putative null	ccatctccaaCCATCGG...CTACAAgaaatctgcc
				ok2892	Deletion	Putative null	caaaaaagcTTCCGAT...AAGCAGGaatgaccaa

∗ Gene is required for presynaptic assembly in AIY

Table S1. Annotated list of autophagy genes examined in this study, related to Figure 2.
List of all of the autophagy genes examined in this study, with corresponding yeast and/or mammalian orthologs (column 1), *C. elegans* names (column 2), examined alleles (column 3), nature of the genetic lesion (column 4), effect on the protein product (column 5), and the change in the genetic sequence (column 6; upper case letters denote deviations from wild type sequence, and "…" denotes missing sequence in the case of large deletions). Asterisk denotes genes that are required for presynaptic assembly in AIY.

Movie S1. Time-lapse video of GFP::LGG-1, AV biogenesis in AIY, related to Figure 5.

Confocal z-stacks were acquired once every 4.4 seconds for 3.3 minutes. Arrows indicate location of autophagosome biogenesis in the synaptic-rich Zone 2 region of the neurite. Corresponds to Figure 5O.

Movie S2. Time-lapse video of GFP::LGG-1, AV biogenesis in AIY, related to Figure 5.

Confocal z-stacks were acquired once every 5.7 seconds for 5 minutes. Arrow indicates location of autophagosome biogenesis in the synaptic-rich Zone 2 region of the neurite. Corresponds to Figure 5.

Movie S3. Time-lapse video of GFP::LGG-1, AV biogenesis in AIY, related to Figure 5.

Confocal z-stacks were acquired once every minute for 18 minutes. Arrow indicates location of autophagosome biogenesis in the synaptic-rich Zone 2 region of the neurite. Corresponds to Figure 5.

Movie S4. Time-lapse video of GFP::LGG-1, AV retrograde trafficking in AIY, related to Figure 5.

Confocal z-stacks were acquired once every 4.3 seconds for 5 minutes. Arrows indicate retrograde autophagosome trafficking events in the AIY neurite. Corresponds to Figure 5P.

Supplemental Experimental Procedures:

Strains and genetics

All worms were cultivated at 20°C on NGM plates seeded with OP50 *E. coli*. As a wild type reference strain, we utilized N2 Bristol worms. We obtained strains harboring the following alleles from the *Caenorhabditis* Genetics Center: *unc-51/atg-1(e369), atg-4.1(gk127286), atg-4.2(gk430078), atg-6/bec-1(ok691), atg-6/bec-1(gk202351), atg-9(gk421128), atg-11/epg-7(gk863004), atg-16.1(gk668615), atg-16.2(gk145022), atg-18(gk447069), epg-2(gk104842), unc-104(e1265), sqst-1(ok2869), sqst-1(ok2892), unc-14(e57), unc-116(e2310), unc-16(ju146),* and NM2415 (*jsIs682* [Prab-3::gfp::rab-3; pJM23]). We also obtained alleles from the Hong Zhang laboratory at the Institute of Biophysics, Chinese Academy of Sciences: *atg-2(bp576), atg-3(bp412), atg-5(bp484), atg-7(bp422), lgg-1(bp500), atg-9(bp564), atg-13/epg-1(bp414), epg-8/atg14(bp251), epg-6/WIPI(bp242),* and *epg-9/Atg101(bp320)*. From the Mitani laboratory at the Tokyo Women's Medical University School of Medicine, we obtained: *lgg-2(tm5755), atg-11/epg-7(tm2508), lgg-3/atg12(tm1642), epg-5(tm3425), epg-3(tm5475), mtm-3(tm4475),* and *atg-7(tm2976)*. We obtained CX9797 (kyIs445 [Pdes-2::mCh::rab-3; Pdes-2::sad-1::gfp]) and *kyIs235* [Punc-86::snb-1::yfp] from the Bargmann lab at the Rockefeller University; NC1686 (*wdIs51* [Pf49h12.4::gfp, unc-119 rescue] from the Miller lab at Vanderbilt University; LX837 (*vsIs45* [Ptph-1::gfp]) from the Koelle lab at Yale University; and *wyIs45* [Pttx-3::gfp::rab-3], *wyIs92* [Pmig-13::snb-1::yfp], *wyIs93* [Pglr-3::glr-1::gfp; Pglr-3::mCh::rab-3], *wyIs97* [Punc-86::myr-gfp; Punc-86::mCh::rab-3], *wyEx1266* [Pcex-1::gfp::rab-3, Phlh-17::mCh], and *wyEx1194* [Pttx-3::unc-40::gfp, Pttx-3::mCh::rab-3] from the Shen lab at Stanford University. Specific allele lesion information can be found in Table S1.

Molecular biology and transgenic lines

We created pSM vector-derived plasmids (Shen and Bargmann, 2003) and transgenic strains (injected at concentrations 0.5-40ng/µl) using standard techniques. We coinjected relevant plasmids with markers *Punc-122::gfp, Punc-122::dsRed, Podr-1::gfp,* or *Podr-1::rfp* (15- 40ng/µl) and generated the following transgenic strains: *olaEx1247* [Pttx-3::atg-9::gfp, Pttx-3::mCh::rab-3], *olaEx2266* [Pttx-3::mCh::rab-3], *olaEx2263* [Pttx-3::mCh::rab-3, Punc-14::atg-9::gfp], *olaEx2091* [Pttx-3::rfp, Pglr-3::rfp, Fosmid WRM0617aE11], *olaEx2169* [Pttx-3::rfp, Pglr-3::rfp, Patg-2::atg-2], *olaEx2281* [Punc-14::atg-9, Pttx-3::mCh, Pglr-3::mCh], *olaEx2188* [Pttx-3::rfp, Pglr-3::rfp, Fosmid WRM0616aF03], *olaEx2119* [Punc-14::lgg-1], *olaEx2113* [Patg-2::atg-2], *olaEx1878* [Pttx-3::gfp:lgg-1, Pttx-3::mCh], *olaEx2558* [Pttx-3::gfp::lgg-1(G116A), Pttx-3::mCh], *olaEx2264* [Punc-14::atg-9::gfp, Pttx-3::mCh::rab-3], *olaEx2226* [Pdes-2::mCh], *olaEx2233* [Pdes-2::mCh::rab-3, Pdes-2::atg-9::gfp], *olaEx2221* [Patg-9(1.9kB upstream)::atg-9 genomic (first 6.4kB)::SL2::gfp, Pttx-3::mCh], *olaEx2191* [Patg-2::gfp, Pttx-3::mCh], *olaIs35* [Pttx-3::gfp::lgg-1, Pttx-3::mCh], *olaEx2935* [Pmod-1::gfp::lgg-1, Pttx-3::mCh], *olaEx2996* [Pmod-1::gfp::lgg-1(G116A), Pttx-3::mCh], *olaEx1972* [Ptph-1::cat-1::gfp, Pthp-1::mCh::rab-3], and *olaEx2045* [Ptph-1::gfp::rab-3, Ptph-1::mCh].

Other strains used in this study include: *olaEx866* [Pttx-3::snb-1::yfp, Pttx-3::mCh::rab-3], *olaIs10* [Pttx-3::gfp::syd-1, Pttx-3::mCh::rab-3], *olaEx294* [Pttx-3::UtrCH::gfp], *olaEx324* [Pttx-3::mig-10B::gfp], *olaIs12* [Phlh-17::CD4::gfp(1-10), Pttx-3::CD4::gfp(11), Pttx-3::mCh::rab-3], *olaEx586* [Pttx-3::gfp, Phlh-17::mCh], and *olaEx791* [Ptph-1::mCh, Ptph-1::gfp::syd-1].

Comprehensive construct and strain information is available upon request.

We amplified *atg-9* and *lgg-1* cDNA by PCR from a pool of cDNA from a mixed-stage population of animals. We used a CRISPR protocol (Dickinson et al., 2015) to create *atg-9(ola270[atg-9::gfp::SEC])*, in which the eGFP coding sequence and the self-excision cassette are inserted in place of the *atg-9* stop codon, and *atg-9(ola274[atg-9::gfp])*, in which the self-excision cassette is excised.

Fluorescence microscopy and confocal imaging

We used 40x Plan Fluor, NA 1.3, and 60x CFI Plan Apo VC, NA 1.4, oil objectives on an UltraView VoX spinning disc confocal microscope on a NikonTi-E stand (PerkinElmer) with a Hammamatsu C9100-50 camera to image fluorescently tagged fusion proteins (eGFP, GFP, YFP, RFP, and mCherry with excitation wavelengths of 488 or 561 nm) and transmitted light in live *C. elegans* at room temperature. We immobilized worms using 10mM levamisole (Sigma) and imaged on 2% agarose pads. We used Volocity software (Improvision by Perkin Elmer) to acquire and process images, using "Extended Focus" to show images as maximal projections. Additional processing of images, such as rotations, cropping, and brightness levels, was conducted with Adobe Photoshop CS4 and Fiji (Schindelin et al., 2012), and figures were assembled with Adobe Illustrator CS4 (Adobe Systems Incorporated). We

performed all quantifications on maximal projections of raw data and all images are oriented anterior to the left and dorsal up.

Mosaic Analysis

We performed mosaic analyses on *atg-9(bp564)*, *lgg-1(bp500)* and *atg-2(bp576)* mutant animals by expressing unstable transgenes with an appropriate rescuing construct and cytoplasmic markers in RIA and AIY (*olaex2281*, *olaEx2091* and *olaEx2169)* as previously described (Colón-Ramos et al., 2007; Herman, 2007; Yochem and Herman, 2003). We used a Leica DM5000 B microscope to analyze mutant animals for presence of the transgene as defined by presence of cytoplasmic RFP in AIY and/or RIA. For each condition, we scored the percentage of worms with rescued AIY presynaptic pattern.

SNP Mapping and Whole-Genome Sequencing

We isolated *atg-9(wy56)* from visual forward-genetic ethyl methanesulfonate (EMS) mutagenesis screens designed to identify mutants that displayed abnormal AIY synaptic vesicle patterning (visualized with GFP::RAB-3). We used single-nucleotide polymorphism (SNP) mapping as described (Davis and Hammarlund, 2006; Davis et al., 2005) to map *wy56* to an interval between 0.005 Mb and 0.5 Mb on chromosome V.

We then performed whole-genome sequencing at the Yale Center for Genome Analysis (YCGA) on *wy56* animals as described (Bigelow et al., 2009; Sarin et al., 2008). We analyzed the data using MaqGene software and confirmed lesions by Sanger sequencing.

Electron Micrographs

We surveyed hundreds of high magnification electron micrographs from the archives of the Center for *C. elegans* Anatomy (Hall lab) to look for evidence of autophagy in embryonic neurons. The archive includes images contributed by Richard Durbin, John White (MRC/LMB, Cambridge) and Carolyn Norris (Hedgecock lab), many of which are publically available on www.WormImage.org. Neuronal autophagic vacuole-like organelles were identified as previously described (Bunge, 1973; Hernandez et al., 2012; Melendez et al., 2003; Yu et al., 2004). Autophagosomes in *C. elegans* are relatively small, owing to the small size of nematode cells (Melendez et al., 2003). We include the provenance of selected micrographs in the Figure legends.

AIY and PVD Quantifications

AIY presynaptic defect

To quantify the penetrance of the AIY presynaptic defect, we used the integrated transgenic line *wyIs45* in the specified mutant backgrounds and quantified penetrance as previously described (Colón-Ramos et al., 2007; Stavoe et al., 2012; Stavoe and Colón-Ramos, 2012). Briefly, Zone 2 was defined morphologically as the region of the AIY process, which turns dorsally from the anterior ventral nerve cord into the nerve ring in adult animals (approximately 5 μm in length at the young adult stage, and highlighted with a dashed box in AIY figures). We defined Zone 3 as the region of the AIY process dorsal to Zone 2 that extends to the end of the dorsal midline. These anatomical definitions were based upon EM reconstruction micrographs (White et al., 1986). We then scored the number of animals displaying normal or abnormal Zone 2 synaptic patterns relative to wild type animals.

To quantify the penetrance of the AIY presynaptic defect in the L1 larval stage, we performed an egg lay as described (Porta-de-la-Riva et al., 2012) and examined resulting progeny after 14-18 hours for AIY presynaptic defects.

We quantified rescue of AIY presynaptic assembly in autophagy mutants by scoring the number of animals displaying a wild type localization pattern of GFP::RAB-3 or mCh::RAB-3 in AIY Zone 2 as described (Colón-Ramos et al., 2007; Stavoe et al., 2012; Stavoe and Colón-Ramos, 2012).

GFP::Rab-3 Enrichment in AIY

To quantify the enrichment of GFP::RAB-3 in AIY Zone 2, we measured the total fluorescence intensity across the AIY Zone 2 and Zone 3 regions in confocal maximal projection micrographs. Enrichment was defined as the total fluorescence intensity of Zone 2 divided by the total fluorescence intensity of both Zones 2 and 3. Fluorescence intensity (after background subtraction) was determined by tracing the AIY neurite using the line scan function in

FIJI (Schindelin et al., 2012). For this quantification, Zone 2 was defined as 20% of the length of the entire AIY synaptic region (Zones 2 and 3).

F-actin Enrichment in AIY

To quantify the penetrance of F-actin enrichment, we used the extrachromosomal transgenic line *olaEx294* (Stavoe and Colón-Ramos, 2012). We scored the number of animals displaying a lack of enrichment of UtrCH::GFP in AIY Zone 2 relative to wild type animals, as described (Stavoe and Colón-Ramos, 2012).

GFP::LGG-1 in AIY

The GFP::LGG-1 probe used in these studies is the same one that has been validated in *C. elegans* by immuno-labeling electron microscopy studies with both anti-GFP and anti-LGG-1 and used to examine the *in vivo* dynamics of autophagosomes in hypodermal seam cells and early embryos (Manil-Segalen et al., 2014; Melendez et al., 2003; Tian et al., 2010; Zhang et al., 2015).To quantify the penetrance of autophagosome (GFP::LGG-1) puncta in the AIY neurite, we used the extrachromosomal array *olaEx1878* [Pttx-3::gfp::lgg-1, Pttx-3::mCh] and scored for presence or absence of LGG-1 puncta in the AIY neurite. We only scored animals where GFP signal could be detected in AIY. In wild type worms (n=169), 73% of animals had GFP::LGG-1 signal in AIY. We also note that although the same extrachromosomal transgenic line was used in different mutant backgrounds, GFP::LGG-1 signal was more prevalent in autophagy mutants as compared to wild type animals, with signal observed in 99% of *atg-3(bp412)* mutants, 100% of *atg-9(bp564)* mutants, 89% of *atg-2(bp576)* mutants, 100% of *epg-6(bp424)* mutants, 99% of *epg-5(tm3425)* mutants, 86% of *atg-2(bp576);unc-104(e1265)* double mutants, and 98% of *epg-6(bp424);unc-104* double mutants, (n>100 for all groups). The absence of signal in 27% of wild type worms likely represents active autophagy degrading the LGG-1 associated with autophagosomes. For the same quantification in the 3-fold embryo, we used *olaEx2935* [Pmod-1::gfp::lgg-1, Pttx-3::mCh] and *olaEx2996* [Pmod-1::gfp::lgg-1(G116A), Pttx-3::mCh] to score for presence or absence of LGG-1 puncta at Zone 2.

We used *olaIs35* [Pttx-3::gfp::lgg-1, Pttx-3::mCh] to quantify the dynamics of LGG-1. For the rates of autophagosome biogenesis, we captured confocal micrographs (z-stacks) once every minute for 30 minutes. A total of 82 time-lapse videos were captured for wild type and mutant animals. We counted the number of GFP::LGG-1 puncta that appeared within the movie, for wild type (n=22 neurons), *atg-9(wy56)* (n=20 neurons), *atg-2(bp576)* (n=20 neurons), *epg-6(bp424)* (n=20 neurons), *epg-5(tm3425)* (n=20 neurons), *unc-104(e1265)* (n=19 neurons), *atg-2(bp576);unc-104(e1265)* (n=19 neurons), and *epg-6(bp424);unc-104(e1265)* (n=19 neurons) mutant animals and report these as biogenesis events in Figure 5N.

To quantify the directionality of autophagosome trafficking, confocal micrographs 57 time-lapse videos (z-stacks) were acquired at maximum speed (imaging at least once every 10 seconds) for 5 minutes, and GFP::LGG-1 puncta were scored as either stationary, moving anterograde (away from the cell body) or retrograde (toward the cell body).

PVD Axon Length

We measured the PVD axon length along the ventral nerve cord (which does not include the distance between the cell body and the ventral nerve cord) using ImageJ software (Schneider et al., 2012).

Glia morphology and visualization of AIY:glia contact

To visualize glia morphology, we used the *hlh-17* promoter driving cytoplasmic mCherry, which expresses in the ventral cephalic sheath cells (VCSC) glia (McMiller and Johnson, 2005). To analyze the AIY-glia contact area, we used GFP reconstitution across synaptic partners (GRASP) (Feinberg et al., 2008), and expressed CD4::GFP 11 in AIY using the *ttx-3* promoter and CD4::GFP(1-10) in glia using the *hlh-17* promoter, as described (Shao et al., 2013).

Statistical Analyses

To determine statistical significance for categorical data, we used Fisher's exact test. Error bars represent 95% confidence intervals. Statistical significance for continuous data was determined using one-way ANOVA with *post hoc* analysis by Tukey's multiple comparisons test or Student's t-test using PRISM software. Error bars for continuous data were calculated using standard errors of the mean (SEM).

Supplemental References:

Colón-Ramos, D.A., Margeta, M.A., and Shen, K. (2007). Glia promote local synaptogenesis through UNC-6 (netrin) signaling in C. elegans. Science *318*, 103-106.

Feinberg, E.H., Vanhoven, M.K., Bendesky, A., Wang, G., Fetter, R.D., Shen, K., and Bargmann, C.I. (2008). GFP Reconstitution Across Synaptic Partners (GRASP) defines cell contacts and synapses in living nervous systems. Neuron *57*, 353-363.

Hegedus, K., Takats, S., Kovacs, A.L., and Juhasz, G. (2013). Evolutionarily conserved role and physiological relevance of a STX17/Syx17 (syntaxin 17)-containing SNARE complex in autophagosome fusion with endosomes and lysosomes. Autophagy *9*, 1642-1646.

Lu, Q., Yang, P., Huang, X., Hu, W., Guo, B., Wu, F., Lin, L., Kovacs, A.L., Yu, L., and Zhang, H. (2011). The WD40 repeat PtdIns(3)P-binding protein EPG-6 regulates progression of omegasomes to autophagosomes. Developmental cell *21*, 343-357.

Obara, K., Sekito, T., Niimi, K., and Ohsumi, Y. (2008). The Atg18-Atg2 complex is recruited to autophagic membranes via phosphatidylinositol 3-phosphate and exerts an essential function. The Journal of biological chemistry *283*, 23972-23980.

Polson, H.E., de Lartigue, J., Rigden, D.J., Reedijk, M., Urbe, S., Clague, M.J., and Tooze, S.A. (2010). Mammalian Atg18 (WIPI2) localizes to omegasome-anchored phagophores and positively regulates LC3 lipidation. Autophagy *6*, 506-522.

Schaheen, L., Dang, H., and Fares, H. (2006). Basis of lethality in C. elegans lacking CUP-5, the Mucolipidosis Type IV orthologue. Developmental biology *293*, 382-391.

Shao, Z., Watanabe, S., Christensen, R., Jorgensen, E.M., and Colon-Ramos, D.A. (2013). Synapse location during growth depends on glia location. Cell *154*, 337-350.

Stavoe, A.K., Nelson, J.C., Martinez-Velazquez, L.A., Klein, M., Samuel, A.D., and Colón-Ramos, D.A. (2012). Synaptic vesicle clustering requires a distinct MIG-10/Lamellipodin isoform and ABI-1 downstream from Netrin. Genes & development *26*, 2206-2221.

Sun, T., Wang, X., Lu, Q., Ren, H., and Zhang, H. (2011). CUP-5, the C. elegans ortholog of the mammalian lysosomal channel protein MLN1/TRPML1, is required for proteolytic degradation in autolysosomes. Autophagy *7*, 1308-1315.

Tian, Y., Li, Z., Hu, W., Ren, H., Tian, E., Zhao, Y., Lu, Q., Huang, X., Yang, P., Li, X.*, et al.* (2010). C. elegans screen identifies autophagy genes specific to multicellular organisms. Cell *141*, 1042-1055.

Treusch, S., Knuth, S., Slaugenhaupt, S.A., Goldin, E., Grant, B.D., and Fares, H. (2004). Caenorhabditis elegans functional orthologue of human protein h-mucolipin-1 is required for lysosome biogenesis. Proceedings of the National Academy of Sciences of the United States of America *101*, 4483-4488.